Comparison of Sentinel-1 SAR and Sentinel-2 for Assessing Mangrove Aboveground Carbon Stock in Pangpang Bay, East Java, Indonesia

Pattiasina, D. B. M. P.,[1] Kamal, M.[2]* and Farda, N. M.[3]
Department of Geographic Information Science, Universitas Gadjah Mada, Yogyakarta, Indonesia
E-mail: devandrabudi@mail.ugm.ac.id, ORCID ID: 0009-0008-3878-9285,[1]
m.kamal@ugm.ac.id, ORCID ID: 0000-0003-4004-086X[2]
farda@ugm.ac.id, ORCID ID: 0000-0003-4535-5668[3]
Corresponding Author

DOI: https://doi.org/10.52939/ijg.v22i3.4875

Abstract
Mangroves are among the plants that effectively absorb CO_2 compared to other terrestrial vegetation. Monitoring their Aboveground Carbon Stock (AGC) in a specific area is essential for conservation and egological management. This research employed optical and radar imageries to estimate mangrove AGC. The radar can penetrate clouds and vegetation canopies, which will further be compared accordingly. Mangrove AGC in Pangpang Bay Mangrove Forest, East Java Province, Indonesia, was assessed using the polynominal regression model. The findings showed that the band 2 of Sentinel-2 exhibited the maximum accuracy level at 74.40%, accompanied by a standard error of 20.28 ton/ha. In this research, the VV (Vertical-Vertical) backscatter variable, identified as the most effective Sentinel-1 independent variable for estimating carbon stock, had an accuracy rate of 58.54% with a standard error of 32.84 ton/ha. Furthermore, the VV backscatter variable exhibited a higher determination coefficient (R^2 = 0.34) compared to band 2 (R^2 = 0.24), hence serving as the most effective predictor of AGC variations.

Keywords: AGC, Mangroves, Regression Analysis, Sentinel-1, Sentinel-2

1. Introduction

Global warming results from the accumulation of carbon dioxide (CO_2) in the atmosphere. It can lead to the greenhouse effect, elevating the earth's average temperature and eventually causing changes in weather patterns, global glacier melt, and sea level rise [1] and (2]. In order to mitigate the impact of global warming, it is necessary to reduce carbon dioxide levels, one of which is by utilizing carbon-absorbing plants through photosynthesis and sequestration [3]. Mangroves possess the capacity to store carbon in large quantities for extended durations compared to terrestrial forests and vegetated coastal areas [4] and [5]. Therefore, mangroves significantly contribute to carbon sequestration and storage in aboveground biomass (leaves, stems, twigs), belowground biomass (roots), and soil sediments; thus, it is essential to manage and conserve mangrove ecosystems to sustain carbon dioxide absorption [6].

Mangrove carbon stock mapping is important for mangrove ecosystem management and conservation, functioning to identify the ecosystem's carbon storage capacity [7]. The data on carbon storage and uptake estimation can be used for sustainable environmental management as they track the amount of carbon storage and uptake over certain time periods [8]. By using the remote sensing method, this mapping is feasible as it surpasses direct field measurement in effectiveness and efficiency regarding time, cost, and extensive area coverage [5][9] and [10]. In general, passive or optical imagery has been shown to significantly contribute to forest monitoring and evaluation efforts, including the assessment of biomass and carbon stocks [11] and [12]. However, optical images are constrained by cloud interference, particularly in tropical regions during wet seasons, leading to inaccurate pixel values and satellite imagery mapping. Atmospheric dust, vapor, and aerosol particles can also affect the radiometric and the pixel values of the images [13] and [14]. Another factor is the saturation of images' pixel values, whereby the spectral reflectance values lose sensitivity to the biomass vegetation as the estimated biomass in a region is very high [15].

The Normalized Difference Vegetation Index (NDVI) is prone to saturation due to its reliance on the near infrared (NIR), which is sensitive to the biophysical characteristics of vegetation [16] and [17]. As an alternative data for mapping, radar images can be used to overcome cloud and atmospheric barriers in optical imaging. It can traverse clouds and the atmosphere to generate cloud-free images [18]. Synthetic Aperture Radar (SAR), a variant of radar, can also provide three-dimensional data of biophysical parameters, rendering it a viable medium for estimating Aboveground Biomass (AGB) and Aboveground Carbon (AGC) in extensive tropical regions [19].

Based on the previous explanation, active remote sensing may serve as an alternative for estimating AGB while ensuring good accuracy. In addition, research on carbon stock estimation using these data is crucial for assessing the radar's efficacy in estimating AGB compared to optical imagery under similar conditions. Therefore, this research was conducted to compare the accuracy of carbon stock mapping in mangroves using the Sentinel-1 polarization, polarization ratio, radar vegetation index, and multiple bands and vegetation index transformation of Sentinel-2.

2. Materials and Methods

2.1 Research Site

This research was conducted in some areas of Pangpang Bay Mangrove Forest, East Java, Indonesia, encompassing an area of 528.09 ha (Figure 1). As these sites are within a conservation area, the ecosystem remains unspoiled [20]. Sandy and muddy substrates are ideal for the growth of *Rhizophora mucronata*. Moreover, the temperature, pH level, and salinity of the local waters are suitable for the growth of *Rhizophora* and *Avicennia*, with a temperature of 27˚–33˚C, a pH of 6.8–7.4, and salinity of 10–33‰ [21]. There are five families of mangrove vegetation distributed in this forest, including *Sonneratiaceae, Rhizoporaceae, Avicenniaceae, Acanthaceae,* and *Meliaceae.* However, field observations reported no presence of *Acanthaceae* and *Meliaceae* among the five species examined. The mangrove species that were often found include *Rhizophora apiculata, Rhizophora stylosa, Rhizophora mucronata, Brugueira gymnorrhiza, Sonneratia alba, Avicennia marina, Ceriops tagal,* and *Ceriops decandra.* These species can be distinguished by their physical appearance, such as the shape of their leaves, stems, and roots. For example, mangrove species such as *Rhizophora stylosa*, *Rhizophora mucronata*, and *Rhizophora apiculata* are characterized by prop roots, while *Avicennia marina* is characterized by pencil roots and small leaves, unlike *Sonneratia alba*, which has larger pencil roots and wider leaves. Then, the differences between species, based on field observations, serve as the basis for determining the wood density of mangrove vegetation used in biomass and carbon stock calculations. Furthermore, a related mangrove species of small *Nypa fruticans* was also identified in the inner zone.

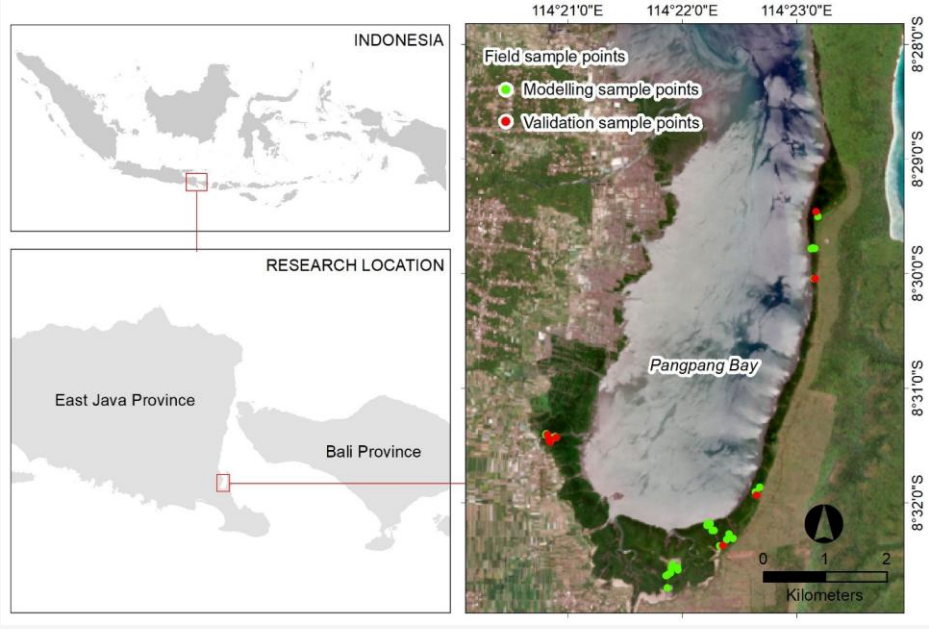

Figure 1: Pangpang Bay mangrove forest, East Java, Indonesia, shown in true color composite of Sentinel-2 image

Table 1: Overview of the satellite imagery

No.	Satellite Imagery	Acquisition Date	Spatial Resolution (m)	Description (Level and Product Type)	ID
1	Sentinel-1	18 November 2023 24 December 2023	10	Ground Range Detected (GRD)	405436 410089
2	Sentinel-2	27 September 2023	10	Level–2A	S2B_OPER_MSI_L2A_DS_S2RP_20241026T073954_S20230927T023803_N05.09

2.2 Data Collection and Preprocessing

This research used Sentinel-1 and Sentinel-2 images obtained from https://scihub.copernicus.eu/, utilizing Sentinel-1 Ground Range Detected (GRD) images and Sentinel-2 level 2A images (Table 1). The Sentinel-2 images used have been adjusted to the Bottom of Atmosphere (BOA) level to generate surface reflectance values [22]. This research utilized two scenes of Sentinel-1 images to correct the multitemporal speckle filtering. This method is effective for Sentinel-1 images since it enhances the spatial detail without significant shifts [23].

2.2.1 Sentinel-1 preprocessing

The correction and calibration of Sentinel-1 images involve four preprocessing stages, *viz.* radiometric calibration, thermal noise removal, multitemporal speckle filtering, and geometric/terrain correction. These stages were processed using SNAP software. The preliminary stage is radiometric calibration to adjust the pixel's backscatter value, thereby accurately representing the actual field conditions [7]. This research used sigma nought calibration for radiometric correction of areas with minimal topographic variations [24] and [25]. The subsequent stage was thermal noise removal correction to eliminate noise resulting from depolarization [26]. After correction, the visual results of the image remained the same, and eventually, the Sentinel-1 images used exhibited minimal thermal noise.

Subsequent to radiometric correction and thermal noise removal, the next stage was speckle filtering. Two pre-corrected Sentinel-1 image scenes were used for multi-temporal speckle filtering using the Frost method. It is among the speckle filtering methods with the smallest Mean Square Error value, leading to a minimal shift of image objects [23]. The final stage was geometric correction to address geometric inaccuracies due to recording effects [27]. With the Range Doppler terrain correction method, which entails the reverse adjustment of each pixel's position to the coordinate point, thereby enabling precise arrangement of pixel values according to the cartographic reference. The researchers used the "convert to dB" feature in the same software to modify the intensity values to correspond with the backscatter ones.

2.2.2 Sentinel-2 preprocessing

The radiometric and geometric corrections are unnecessary as the Sentinel-2 images used in this research are level 2A, with pixel values representing Surface Reflectance (SR). Nevertheless, while the pixel values are in the form of Digital Number (DN) values ranging from 0 to 10,000, they must be converted to object reflectance values ranging from 0 to 1 [28]. This research used merely four of the 13 bands from the Sentinel-2 images (Table 2), including visible blue, green, red, and near-infrared (NIR) bands. This is because the spatial resolution of the image was adjusted to the size of the sample plot used for field measurements, which was 10 x 10 meters.

2.3 Image Variable Processing

Alongside the backscatter and spectral reflectance values of each band, derivative independent variables were also utilized. The variables comprise three polarization transformation results from Sentinel-1 images, one vegetation index from Sentinel-1 images, and six vegetation indices of Sentinel-2 images. In total, there were 16 independent variables used in this research. The radar polarization transformation (Cross Ratio) applied the VH and VV polarization backscatters, which are sensitive to biomass and water content in vegetation [29] and [30]. Therefore, it is applicable to mangrove forests with high water content. Additionally, the polarization division, a highly reliable predictor of biomass [31], and the Radar Vegetation Index (RVI) for Sentinel-1 [32], were also used. The variables for Sentinel-2 imagery comprise the Normalized Difference Vegetation Index (NDVI), Enhanced Vegetation Index (EVI), Difference Vegetation Index (DVI), Soil-Adjusted Vegetation Index (SAVI), Modified Soil-Adjusted Vegetation Index (MSAVI2), and Atmospherically Resistant Vegetation Index (ARVI). Table 3 presents the equations (Equations 1 to 10) used for derivative-dependent variables of Sentinel-1 and Sentinel-2.

Table 2: Spectral bands of Sentinel-2 images

No	Band number	Band description	Central Wavelength (µm)	Spatial Resolution (meter)
1	B1	Band 1 – Coastal aerosol	0.443	60
2	B2	Band 2 – Blue	0.490	10
3	B3	Band 3 – Green	0.560	10
4	B4	Band 4 – Red	0.665	10
5	B5	Band 5 – Vegetation Red Edge	0.705	20
6	B6	Band 6 – Vegetation Red Edge	0.740	20
7	B7	Band 7 – Vegetation Red Edge	0.783	20
8	B8	Band 8 – Near Infrared (NIR)	0.842	10
9	B8A	Band 8A – Vegetation Red Edge	0.865	20
10	B9	Band 9 – Water vapor	0.945	60
11	B10	Band 10 – SWIR – Cirrus	1.375	60
12	B11	Band 11 – SWIR	1.610	20
13	B12	Band 12 – SWIR	2.190	20

Table 3: The independent variables

Image	Variable	Formula	Equation number	Reference
Sentinel-1	Cross Ratio	$\sigma^0_{VH} - \sigma^0_{VV}$	[33]	[33]
	Polarization Division 1	$\sigma^0_{VH} / \sigma^0_{VV}$	[31]	[31]
	Polarization Division 2	$\sigma^0_{VV} / \sigma^0_{VH}$	[31]	[31]
	RVI	$RVI = \frac{4\sigma^0_{VH}}{\sigma^0_{VV} + \sigma^0_{VH}}$	[32]	[32]
Sentinel-2	NDVI	$\frac{NIR - RED}{NIR + RED}$	[34]	[34]
	EVI	$2.5 \times \frac{NIR - RED}{NIR + 6RED - 7.5BLUE + L}$	[35]	[35]
	DVI	$NIR - RED$	[36]	[36]
	SAVI	$\frac{NIR - RED}{NIR + RED + L}(1 + L)$	[37]	[37]
	MSAVI2	$0.5\left(2NIR + 1 - \sqrt{(2NIR+1)^2 - 8(NIR - RED)}\right)$	[38]	[38]
	ARVI	$\frac{NIR - RED - \gamma(BLUE - RED)}{NIR + RED - \gamma(BLUE - RED)}$	[39]	[39]

2.4 Fieldwork and Sampling Method

The field sample points were determined using a purposive sampling method, considering the accessibility of the location, either by land or waterway. This method is both effective and efficient in terms of time, energy, and the optimality of sample size [40]. The sampling activity involved measuring the circumference of mangrove trees to determine the Diameter at Breast Height (DBH) of the trunks, height, and canopy density. The DBH value of the tree trunk can be directly used to calculate the AGB value using the general allometric equation [41]. This equation calculates the top biomass of each tree with a diameter from 5–49 cm and an optimal height under 10 meters [42]. Afterwards, the AGB value was converted into AGC value by assuming that 47% of the total AGB constitutes AGC based on the SNI 7724:2019 on the assessment of forest carbon stocks. In addition, supplementary data, including mangrove species and the coordinates of each sample plot, were also acquired. The sample is a square area of 10 x 10 meters. This sample plot also used on in research to develop an AGC estimation model using Sentinel-2 imagery [43].

The measurement was performed at 41 sites in the Pangpang Bay Mangrove Forest in five days (Figure

1). Terrain accessibility and meteorological changes were among the challenges encountered during the sampling. However, the total of 41 plots was determined based on field accessibility and data representativeness across varying mangrove structures, which is consistent with several recent studies showing that 30–60 plots are generally sufficient for remote sensing–based biomass estimation [44]. Although relatively limited, the number of plots still met the minimum sample range recommended for tropical forest studies, especially when stratified sampling and model validation are applied. Therefore, the 41-plot dataset was considered adequate to ensure statistical robustness while balancing field constraints and model reliability.

The predominant mangrove species in that area is *Ceriops tagal,* situated in the inner zone of the mangrove forest. In addition, carbon stock values under 50 ton/ha were found in the central part of the mangrove forest (Table 4), predominantly characterized by *Ceriops tagal* with a range of carbon stock values from 20.11 to 47.73 ton/ha. From the table of field data collection results above (Table 4), it can be seen that the number of trees in each plot varies, ranging from 4 to 50 trees with an average DBH of 6.3-16.6 cm. The table also shows that there is an inverse relationship between the number of trees and the average DBH, where sample locations with a large average DBH have fewer trees, such as plots 20 and 29, which have average DBHs of 14.79 cm and 16.66 cm, respectively. In locations with a large number of trees, such as plots 6 (40 trees) and 11 (50 trees), the average DBH of the tree trunks was only around 8.99 cm and 8.66 cm, respectively. This could be due to differences in species and competition between trees for sunlight, nutrient supply, and growing space, which inhibited growth.

Table 4: Field collected data

Sample ID	Number of Trees	Average DBH (cm)	Field AGC (ton/ha)	Dominant Species
1	19	9.41	52.62	*R.mucronata*
2	10	12.64	63.14	*R.mucronata*
3	16	11.40	70.20	*R.mucronata*
4	23	8.87	52.79	*R.mucronata*
5	17	10.13	0.09	*R.mucronata*
6	40	8.99	94.46	*C.tagal*
7	46	7.41	66.80	*C.tagal*
8	35	8.88	79.22	*C.tagal*
9	41	8.65	98.67	*C.tagal*
10	27	9.94	87.21	*C.decandra*
11	50	8.66	107.04	*C.tagal*
12	16	12.59	101.12	*R.stylosa*
13	17	8.85	40.42	*R.apiculata*
14	12	14.81	108.57	*R.apiculata*
15	14	10.81	59.43	*R.apiculata*
16	19	9.21	47.85	*R.stylosa*
17	17	8.66	38.42	*R.mucronata*
18	20	9.67	54.50	*R.mucronata*
19	4	13.61	40.75	*R.apiculata*
20	9	14.79	70.11	*R.apiculata*
21	8	14.24	60.90	*R.apiculata*
22	12	11.55	62.25	*R.apiculata*
23	9	8.95	44.07	*X.moluccensis*
24	9	12.28	123.84	*R.apiculata*
25	11	11.76	118.96	*R.apiculata*
26	9	11.54	118.42	*R.apiculata*
27	9	10.93	84.26	*R.apiculata*
28	8	15.58	146.81	*R.apiculata*
29	6	16.66	137.30	*R.apiculata*
30	11	12.62	127.80	*R.apiculata*
31	29	7.42	95.77	*C.tagal*
32	22	7.44	67.74	*C.tagal*
33	23	6.36	48.00	*C.tagal*
34	18	9.23	102.39	*C.tagal*
35	37	7.74	127.68	*C.tagal*
36	37	7.18	106.04	*C.tagal*
37	48	7.52	139.11	*C.tagal*
38	21	7.78	81.57	*C.tagal*
39	21	10.52	156.01	*C.tagal*
40	25	9.61	150.46	*C.tagal*
41	22	13.34	291.81	*C.tagal*

2.5 Modelling the Aboveground Carbon Stock Using Sentinel-1 and Sentinel-2

Of the 41 field samples collected, 31 samples, approximately 75% of the total, were used for modelling, while the remaining were used for accuracy testing. A multivariate regression analysis requires a minimum of 10 samples for each variable of interest [45]. Therefore, a minimum of 30 samples is necessary for conducting a multivariate regression analysis with three variables of interest that contains two independent variables and one dependent variable. The researchers performed a Pearson correlation test and regression analysis to identify the optimal factors among six Sentinel-1 variables and ten Sentinel-2 variables. The correlation test seeks to determine the relationship between the dependent and the independent variables, with the dependent variable being the field carbon stock value represented by the correlation coefficient (r) [46]. The Pearson correlation test generates a Pearson correlation coefficient that indicates a linear relationship between two variables [47]. In addition to the correlation test, regression analysis is also crucial for identifying the most pertinent independent variable related to the dependent variable. Meanwhile, the regression analysis produces a regression equation and a coefficient of determination (R^2), which assess the ability of the independent variable elucidates the dependent variable; ergo, a higher R^2 value indicates a superior explanatory capacity of the independent variable regarding the dependent variable [48].

The regression analysis is non-linear and employes a second-order polynomial, as carbon stock levels may exhibit a non-linear correlation with remote sensing variables [49]. Subsequently, the modelling results were evaluated for accuracy to measure the model's effectiveness in estimating AGC stock. This research employed the Standard Error of Estimate (SEE) method and the 1:1 goodness of fit plot or 1:1 plot for the modelling accuracy test. The SEE method assesses the number of errors in each sample [50], whereas the 1:1 plot evaluates data distribution and quantifies the results of modelling estimates [51]. The accuracy test was conducted using 25% of the total field sample. The workflow in this research can be seen in Figure 2.

3. Results

3.1 Field Aboveground Carbon Stock Calculation

The calculations utilized the generic allometric equation proposed by [41] with stem density coefficients from [52] (Table 5). The result of this calculation yields the aboveground biomass (AGB) of each mangrove stem, which is further converted into carbon stocks in accordance with the SNI 7724:2011 by multiplying the results of the biomass calculation from [41] by 0.47.

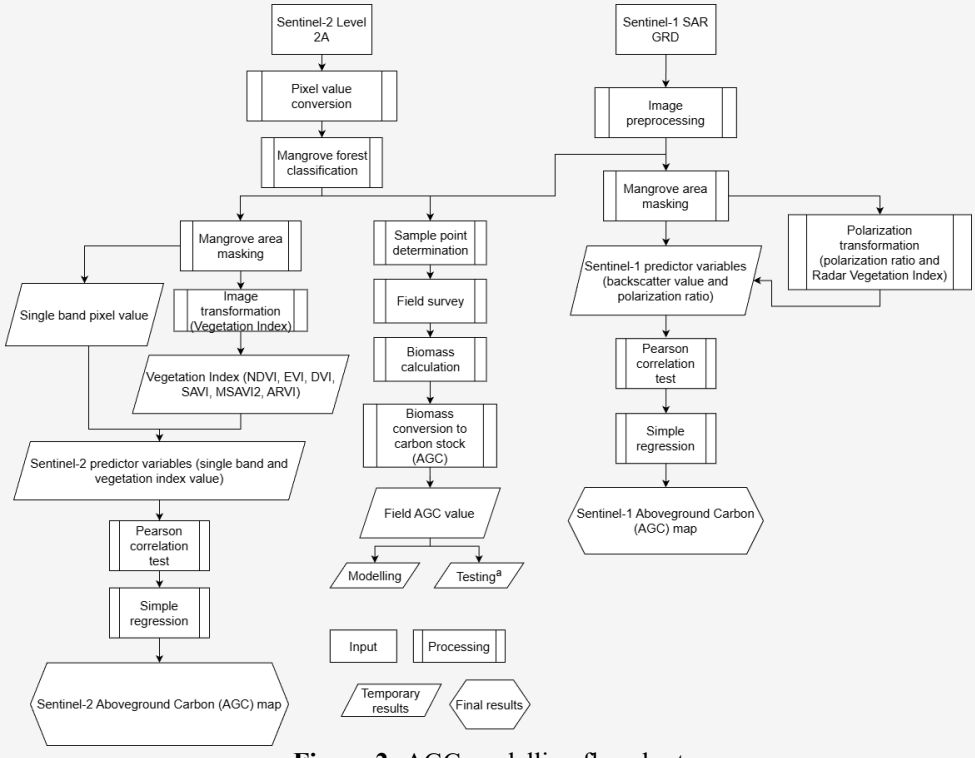

Figure 2: AGC modelling flowchart

Table 5: Wood density of each mangrove species used for AGC calculation

No	Mangrove species	Wood density (g/cm^3)
1	*Ceriops decandra*	0.87
2	*Ceriops tagal*	0.85
3	*Rhizophora apiculata*	0.87
4	*Rhizophora mucronata*	0.83
5	*Rhizophora stylosa*	0.84
6	*Sonneratia alba*	0.47
7	*Xylocarpus moluccensis*	0.65

Table 6: Correlation test results of Sentinel-1 and Sentinel-2 independent variables on field carbon stock values

No		Variable	Pearson Coefficient (r)	Significance
1	Sentinel-1	Backscatter VH	-0.25	0.17
2		**Backscatter VV**	**-0.38**	**0.03**
3		Cross-ratio	0.25	0.18
4		Polarization Division 1	0.34	0.06
5		Polarization Division 2	-0.22	0.22
6		RVI	0.31	0.09
7	Sentinel-2	**B2**	**-0.43**	**0.02**
8		B3	-0.33	0.07
9		B4	-0.32	0.077
10		B8	0.16	0.39
11		NDVI	0.32	0.08
12		SAVI	0.25	0.17
13		MSAVI2	0.24	0.19
14		DVI	0.22	0.24
15		ARVI	0.27	0.14
16		EVI	0.21	0.25

This is due to 47% of the total vegetation biomass composed of carbon. The results showed that the site has a carbon stock value derived from field measurements, ranging from 20.11 to 208.13 ton/ha. Carbon stock values exceeding 100 ton/ha were identified in the eastern part of the mangrove forest, ranging from 108.7 to 208.13 ton/ha. The predominant mangrove species in that area is *Ceriops tagal,* situated in the inner zone of the mangrove forest. In addition, carbon stock values under 50 ton/ha were found in the central part of the mangrove forest, predominantly characterized by *Ceriops tagal* with a range of carbon stock values from 20.11 to 47.73 ton/ha. The stand density in the eastern part of the mangrove forest exceeded that of the western one, presumably resulting in differing carbon values despite species similarity.

3.2 Statistical Analysis for Aboveground Carbon Stock Mapping

A normality test was performed as the early stage of the statistical analysis of the data used for AGC mapping, comprising field AGC calculation data and pixel/backscatter values of Sentinel-1 and Sentinel-2 images. The normality test was done using the Shapiro-Wilk method, yielding a value of 0.34 which indicates that the data can be regarded as normally distributed, allowing for the subsequent correlation test. The Pearson correlation test indicated a negative relationship between the single band Sentinel-2 imagery and the field carbon stocks. Band 2 of Sentinel-2 imagery exhibited the highest correlation coefficient among all independent variables, recorded at -0.43, followed by the VV backscatter of Sentinel-1 imagery at -0.38 (Table 6). Both of these variables had significance values under 0.05. They are statistically significant variables and can be used for modelling. The relatively low correlation coefficient between the two variables may result from saturation in the spectral values of the satellite images. Spectral saturation may transpire at biomass or carbon stock values above 156 ton/ha [53]. A comparable effect was also observed in research, where spectral saturation led to a lower coefficient of determination *(R^2)* for estimating mangrove AGC, with values of 0.22 on Sentinel-2 and 0.11 on Sentinel-1 [7]. This saturation affects the sensitivity of satellite imagery in estimating carbon stocks, particularly in high canopy-density forests [17].

3.3 Mangrove Aboveground Carbon Stock Mapping

3.3.1 Mangrove aboveground carbon stock mapping using Sentinel-1

Active system remote sensing imagery, such as Sentinel-1 SAR, is applicable for estimating and mapping mangrove AGC due to its ability to penetrate clouds and its sensitivity to surface roughness, dielectric constant, and humidity of objects [54] and [55]. Subsequently, the SAR backscatter value was employed as an AGC estimator by extrapolation based on the results of the field AGC calculation. The field AGC value, as the dependent variable, is linked to the field AGC value using correlation test and regression analysis. The results showed that the VV backscatter has a coefficient of determination (R^2) of 0.37 in non-linear polynomial regression. Since the regression analysis used is a non-linear regression, the modelling is site-specific; therefore, it is essential to adjust the data to enable the model's application in other locations. The coefficient of determination indicates that the AGC estimation model using Sentinel-1 VV backscatter can accurately account for 36.91% of the variation in AGC values. The model exhibited AGC values ranging from 50.04 to 454.73 ton/ha, with a mean estimate of 68.96 ton/ha (Table 7). Furthermore, the modelling also estimated a total AGD of 36,180 ton across the research sites including over 500 hectares. Afterwards, the VV backscatter estimations were categorized into five AGC value groups for mapping, including 40 ton/ha, 40 – 60 ton/ha, 60 – 80 ton/ha, 80 – 100 ton/ha, and > 100 ton/ha (Figure 3(a)). The estimations predominantly yielded AGC values within the 40 – 60 ton/ha. The highest AGC values were located in the center of the mangrove forest and the landward zone. In the eastern and western parts of the forest, *viz.* in the peripheral or coastal zone, AGC values were anticipated to exceed 100 ton/ha. The visual disparity in AGC values derived by zonation with VV backscatter is notably imprecise, particularly inside the central and inner zones.

3.3.2 Mangrove aboveground carbon stock mapping using Sentinel-2

Similar to AGC mapping accomplished with Sentinel-1 SAR, the AGC mapping using Sentinel-2 imagery was performed through non-linear polynomial regression analysis. The modelling of the AGC estimate using Sentinel-2 Band 2 resulted in an R^2 value of 0.24. This indicates that 24.03% of the variation in AGC values may be accurately elucidated by this model.

Table 7: Statistical results of AGC modelling

No	Statistic	Backscatter VV	Band 2
1	Min	50.04	25.31
2	Max	454.73	400.29
3	Mean	68.96	63.64
4	Std. Dev.	36.24	26.03

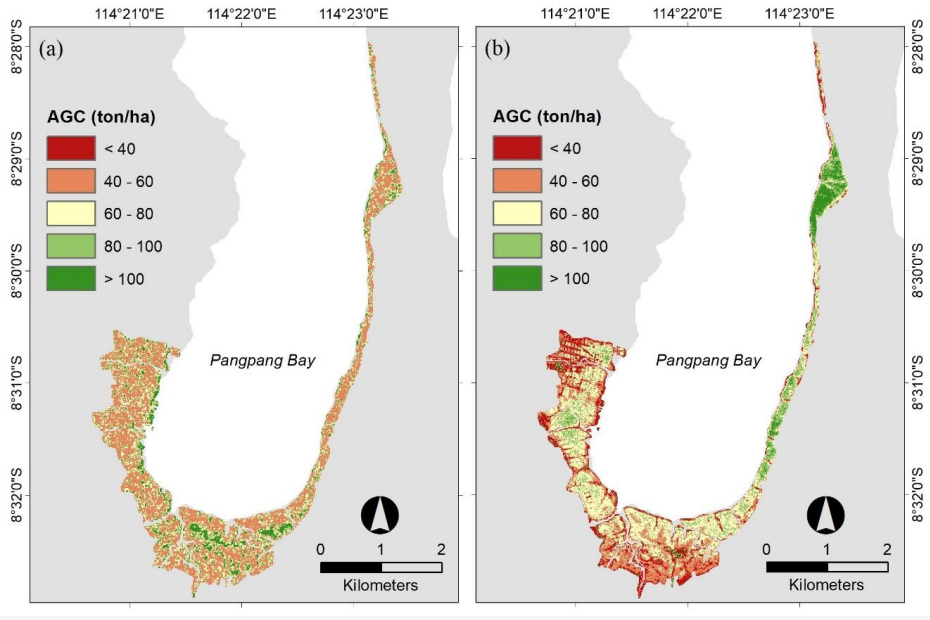

Figure 3: AGC maps produced from: (a) Sentinel-1 VV backscatter and (b) Sentinel-2 band 2

The value was lower than the Sentinel-1 VV backscatter AGC modelling. This model generated AGC values ranging from 25.31 to 400.29 ton/ha. Although the range of AGC values in this model was more constrained than that of the Sentinel-1 modelling, it yielded a lower average AGC estimate of 63.64 ton/ha (Table 6). Furthermore, the model produced a total AGC of 33,593 ton of carbon, which is lower than that of the Sentinel-1 model.

Meanwhile, similar to AGC estimation using VV backscatter, the AGC estimation using Sentinel-2 band 2 was categorized into the identical five AGC value groups for mapping (Figure 3(b)). There is a difference in the spatial distribution of AGC values in this modelling, with the seaward zone of the western mangrove forest categorized under the low AGC value class (≤ 40 ton/ha), whereas the highest AGC value class was located in the middle zone of the eastern mangrove forest. In the central part of the mangrove forest, the estimated AGC values predominantly ranged from 40 to 60 ton/ha in the landward zone and from 60 to 80 ton/ha in the middle and outer zones. The use of band 2 distinctly showed the disparity in AGC values between zones, in contrast to utilizing VV backscatter. The band 2 modelling results indicated that the western part, formerly a pond, exhibited a relatively low AGC value compared to other natural parts of the forest.

3.4 Accuracy Assessment of Mangrove Aboveground Carbon Stock Mapping

This research employed two steps to assess the performance of AGC estimation modelling, including the Standard Error of Estimate (SEE) accuracy test and the 1:1 plot. The accuracy test was conducted using ten samples of AGC values derived from field measurements. The SEE accuracy test indicated that both modelling results achieved an accuracy exceeding 50%, with the Sentinel-2 band 2 AGC modelling demonstrating higher accuracy compared to the Sentinel-1 VV backscatter AGC modelling, yielding accuracy test values of 74.40% and 58.54%, respectively (Table 8). The results of the accuracy test did not correlate with the model's capacity to explain the variation of the AGC value, as indicated by the R^2 value. This suggests that the model derived from Sentinel-2 band 2 exhibits higher accuracy, despite its diminished capacity to explain variations in AGC values compared to the model from Sentinel-1 VV backscatter. The lower Standard Error (SE) value of Sentinel-2, at 20.28, compared to Sentinel-1's 32.84, demonstrated that the band 2 model more accurately reflects the actual AGC values.

The accuracy test of the 1:1 plot method indicated that the band 2 model exhibited greater consistency than the VV backscatter model. This can be seen in Figure 4 where the points on the 1:1 band 2 plot exhibit clustering and alignment with the 1:1 line, in contrast to the 1:1 VV backscatter plot, which shows greater dispersion. The 1:1 band 2 plot also demonstrated that the model had a tendency for overestimation, with eight AGC field sample points overestimated and two sample points underestimated. Nonetheless, one sample point with an estimation result nearly approximating the actual data was the AGC value of 101 ton/ha. Furthermore, the band 2 model also had a higher saturation threshold compared to the VV backscatter model, with saturation occurring at a field AGC value of 90 ton/ha for band 2, whereas the VV backscatter model reached saturation at 66 ton/ha. This suggests that the VV backscatter model is suboptimal in estimating AGC with a high actual AGC value.

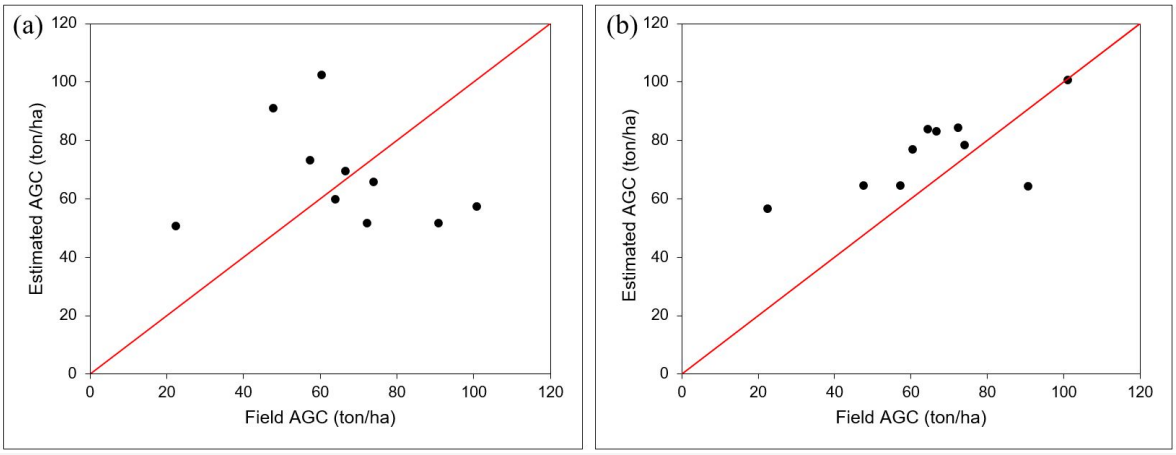

Figure 4: Plot of 1:1 for AGC modelling; (a) backscatter VV and (b) band 2

Table 8: Results of AGC modelling SEE accuracy test

No	Statistic	Backscatter VV	Band 2
1	SE (ton/ha)	32.84	20.28
2	Min Accuracy (%)	58.54	61.12
3	Max Accuracy (%)	37.02	74.40

4. Discussion

The Sentinel-1 VV Backscatter and Sentinel-2 Band 2 variables effectively estimated the AGC of mangrove vegetation in this research. In fact, compared to other variables, including other single bands (band 3, band 4, band 5, and band 8) and vegetation indices used in this research, band 2 emerged as a statistically significant variable, as evidenced by the preceding Pearson correlation test which showed that band 2 was the sole Sentinel-2 variable with a significance value below 0.05. Likewise, the Sentinel-1 VV backscatter variable was the sole variable exhibiting a significance value below 0.05. These two variables are applicable for mangrove AGC modelling using regression analysis. The correlation test results indicated that the Sentinel-2 band 2 variable had a superior relationship compared to the Sentinel-1 VV backscatter variable, despite the inverse nature of this association. Band 2 has a negative Pearson correlation coefficient (r = -0.68) with the actual mangrove AGC value [43]. This also occurs in other visible wave bands, such as band 3 (green visible band) and band 4 (red visible band). This inverse relationship occurs due to the absorption of electromagnetic energy by the leaves, so that an increase in biomass or AGC value at a location corresponds to an increase in energy absorption.

The chlorophyll in leaves absorbs the most electromagnetic energy at a wavelength of 420 nm, while carotenoids absorb most effectively at a wavelength of 445 nm [56]. These wavelengths are situated in the blue visible wave spectrum, hence the incorporation of biomass or AGC into vegetation increases the absorption of electromagnetic waves in this spectrum due to increased vegetation density. The adverse correlation was also evident in the results of the VV backscatter correlation test, which indicates an inverse relationship between the backscatter value and field AGC. A comparable phenomenon was also observed in research [57], which identified a negative correlation between aboveground biomass (AGB) and Sentinel-1 VV and VH backscatter values.

The regression analysis results showed that the VV backscatter variable outperformed the band 2 variable in modelling mangrove AGC. This was indicated by the higher R^2 value of VV backscatter (R^2 = 0.37) compared to band 2 (R^2= 0.24), suggesting that the VV backscatter is more effectively elucidates variations in mangrove AGC values. This was also reinforced by the regression graph modelling AGC band 2 and VV backscatter (Figure 4), where the VV backscatter had a more diffuse distribution of sample points in contrast to the one in the band 2 regression graph. This makes Sentinel-1 potentially usable in AGC estimation at locations with high variations in AGC values. This analysis produces AGC estimation modelling using Sentinel-1 SAR VV backscatter and band 2 Sentinel-2 imagery, which will further be compared in terms of accuracy and spatial distribution.

AGC modelling using Sentinel-2 band 2 produced a broader range of AGC values compared to AGC modelling using Sentinel-1 VV backscatter. However, the average AGC value estimated using the VV backscatter was higher than that modelled using band-2. This is because the minimum and maximum AGC values estimated using VV backscatter were higher than those estimated using band 2. In addition, the degree of variation in AGC values in the VV backscatter modelling was higher than that in band 2, as indicated by the larger standard deviation. This suggests that the VV backscatter has significantly higher data heterogeneity than band 2.

The modelling accuracy test results showed that both models exhibited commendable accuracy, with a Standard Error (SE) of 32.84 ton/ha for the VV backscatter model and 20.28 ton/ha for the band 2 model (Table 8). The AGC of mangroves in the Bedul Mangrove Forest, located in Alas Purwo Forest, Banyuwangi Regency was estimated using Planetscope imagery and produced models with SE values ranging from 31.41 to 32.93 ton/ha [40]. This indicates that VV and band 2 backscatter can optimally estimate mangrove AGC. Furthermore, the accuracy of both models reached 74.4% for band 2 and 58.54% for VV backscatter. The accuracy test results in this research also showed that band 2 was more accurate in modelling mangrove AGC compared to VV backscatter, as evidenced by the more consistent distribution of 1:1 plot point in the band 2 model compared to those in the VV backscatter model.

Although the VV modeling results have a higher R^2 value than Band 2, this model still has a lower prediction accuracy level as indicated by a smaller standard error value. This also shows that the R^2 value is not aligned with the SE value, as R^2 only indicates the statistical influence between variables without providing an estimation accuracy value [58].

Therefore, it is necessary to evaluate the model using error-based measurements such as the Standard Error of Estimate (SEE), which describes how accurate the model is in estimating the AGC value, which is then used as a reference to determine the most optimal final model.

The modelling produced a total AGC stocks of 36,180 ton in the Sentinel-1 modelling and 33,593 ton in the Sentinel-2 modelling. In comparison to other mangrove forest areas in Java, including the Clungup Mangrove Conservation in Malang (3,834 ton) [59], the total AGC at the research site was superior, with average AGC estimates of 63.64 ton/ha (band 2) and 68.96 ton/ha (VV backscatter), exceeding the 47.34 ton/ha benchmark. Nevertheless, when compared to the total and average AGC in Karimunjawa Island [5], the total and average AGC in Pangpang Bay Mangrove Forest is inferior to both sites. Karimunjawa Island has a total AGC stocks of 96,482 ton, encompassing an area of approximately 440 ha (average AGC stocks of 216.4 ton/ha). Another research. reported that the total AGC stocks in Benoa Bay Mangrove Forest, Bali reached 35,349.87 ton/ha over an area of 391.85 ha [60]. Although the total AGC value was lower than that of Pangpang Mangrove Forest, the average AGC at this site was higher, reaching 90.21 ton/ha.

5. Conclusions

The AGC estimation mapping using Sentinel-1 and Sentinel-2 images in this study was conducted using Sentinel-1 VV backscatter and Sentinel-2 band 2 with non-linear regression analysis. The modelling achieved commendable accuracy, with Standard Error values of 32.84 ton/ha for the VV backscatter (maximum accuracy of 58.54%) and 20.28 ton/ha for band 2 (maximum accuracy of 20.28 ton/ha). Nonetheless, the VV backscatter accounted for variations in AGC values more effectively than band 2, as evidenced by the regression analysis results indicating that the VV backscatter ($R^2 = 0.37$) had a higher R^2 value than band 2 ($R^2 = 0.24$).

The higher explanatory power of Sentinel-1 VV backscatter reflects its sensitivity to vegetation structure and its independence from atmospheric conditions, making it particularly suitable for AGC mapping in cloud-prone tropical regions. In contrast, Sentinel-2 band 2, operating in the visible spectrum, is more affected by atmospheric interference and saturation in dense vegetation, limiting its effectiveness. Despite these results, the relatively moderate R^2 values suggest that AGC estimation remains influenced by complex biophysical factors not fully captured by single-band data.

Overall, the findings underscore the importance of radar-based observations for regional AGC mapping and highlight the need for integrating multi-band optical data, multi-polarization SAR, and advanced modelling approaches to further improve estimation accuracy and support robust carbon monitoring.

Acknowledgments

The authors would like to thank (1) the Department of Geographic Information Science, Faculty of Geography, Universitas Gadjah Mada for providing research facilities and equipment, (2) Alas Purwo National Park and Perum Perhutani Blambangan for granting research permission in Pangpang Bay Mangrove Forest, and (3) G. B. Adidharma, A.R. Salsabilla, B.A. Anggarifta, G. Akbar, and Y.A. Jabbar for implementing field research.

References

[1] Anurogo, W., Sari, L. R., Lubis, M. Z., Pamungkas, D. S., Mufida, M. K. and Lestari Situmorang, A. D., (2018). An Integrated Comparative Approach to Estimating Forest Aboveground Carbon Stock Using Advanced Remote Sensing Technologies. *2018 International Conference on Applied Engineering (ICAE)*, Batam, Indonesia, 4-8 October 2018. 1–6. https://doi.org/10.1109/INCAE.2018.8579375.

[2] Abbass, K., Qasim, M. Z., Song, H., Murshed, M., Mahmood, H. and Younis, I., (2022). A Review of the Global Climate Change Impacts, Adaptation, and Sustainable Mitigation Measures. *Environmental Science and Pollution Research*, Vol. 29(28); 42539–42559. https://doi.org/10.1007/s11356-022-19718-6.

[3] Chen, Y., Feng, X., Tian, H., Wu, X., Gao, Z., Feng, Y., Piao, S., Lv, N., Pan, N. and Fu, B., (2021). Accelerated Increase in Vegetation Carbon Sequestration in China After 2010: A Turning Point Resulting from Climate and Human Interaction. *Global Change Biology*, Vol. 27(22); 5848–5864. https://doi.org/10.1111/gcb.15854.

[4] Nellemann, C., Corcoran, E., Duarte, C. M., Valdés, L., De Young, C., Fonseca, L. and Grimsditch, G. (Eds)., (2009). *Blue Carbon. A Rapid Response Assessment*. United Nations Environment Programme, GRID-Arendal, www.grida.no.

[5] Wicaksono, P., Danoedoro, P., Hartono, and Nehren, U., (2016). Mangrove Biomass Carbon Stock Mapping of the Karimunjawa Islands Using Multispectral Remote Sensing. *International Journal of Remote Sensing*, Vol.

37(1); 26–52. https://doi.org/10.1080/01431161.2015.1117679.

[6] Kauffman, J. B. and Donato, D. C., (2012). *Protocols for The Measurement, Monitoring and Reporting of Structure, Biomass and Carbon Stocks in Mangrove Forests*. Working Paper 86. CIFOR, Bogor, Indonesia. https://www.cifor-icraf.org/publications/pdf_files/WPapers/WP86CIFOR.pdf.

[7] Hakim, M. A., Kamal, M. and Arjasakusuma, S., (2022). Mapping Mangrove Surface Carbon Stocks Using Multisensor Imagery in Clungup Mangrove Conservation (CMC) Malang Regency. *Jurnal Geografi*, Vol. 14(2); 192-201. https://doi.org/10.24114/jg.v14i2.33575.

[8] Oktaviani, D., Sunardi, and Sumiarsa, D., (2024). Carbon Stock of Mangrove Ecosystem and Role Blue Economy in Pangandaran West Java. *E3S Web of Conferences*, Vol. 495. https://doi.org/10.1051/e3sconf/202449502002

[9] Argamosa, R. J. L., Blanco, A. C., Baloloy, A. B., Candido, C. G., Dumalag, J. B. L. C., Dimapilis, L. L. C. and Paringit, E. C., (2018). Modelling Above Ground Biomass of Mangrove Using Sentinel-1 Imagery. *ISPRS Annals of the Photogrammetry, Remote Sensing and Spatial Information Sciences*, Vol. 4(3); 13–20. https://doi.org/10.5194/isprs-annals-IV-3-13-2018.

[10] Pham, T. D., Xia, J., Thang Ha, N., Tien Bui, D., Nhu Le, N. and Tekeuchi, W., (2019). A Review of Remote Sensing Approaches for Monitoring Blue Carbon Ecosystems: Mangroves, Sea Grasses and Salt Marshes During 2010–2018. *Sensors*, Vol. 19(8). https://doi.org/10.3390/s19081933.

[11] Huang, X., Ziniti, B., Torbick, N. and Ducey, M. J., (2018). Assessment of Forest Above Ground Biomass Estimation Using Multi-Temporal C-band Sentinel-1 and Polarimetric L-band PALSAR-2 Data. *Remote Sensing*, Vol. 10(9). https://doi.org/10.3390/rs10091424.

[12] Santoro, M. and Cartus, O., (2018). Research Pathways of Forest Above-Ground Biomass Estimation Based on SAR Backscatter and Interferometric SAR Observations. *Remote Sensing*, Vol. 10(4). https://doi.org/10.3390/rs10040608.

[13] Rumora, L., Miler, M. and Medak, D., (2021). Contemporary Comparative Assessment of Atmospheric Correction Influence on Radiometric Indices Between Sentinel-2A and Landsat 8 Imagery. *Geocarto International*, Vol. 36(1); 13–27. https://doi.org/10.1080/10106049.2019.1590465.

[14] Takemura, T., (2023). Radiative Forcing of Particulate Matters. Handbook of Air Quality and Climate Change, H. Akimoto, H. Tanimoto, eds. Singapore: Springer. 1031–1043. https://doi.org/10.1007/978-981-15-2760-9_31.

[15] Zhao, P., Lu, D., Wang, G., Liu, L., Li, D., Zhu, J. and Yu, S., (2016). Forest Aboveground Biomass Estimation in Zhejiang Province Using the Integration of Landsat TM and ALOS PALSAR Data. *International Journal of Applied Earth Observation and Geoinformation*, Vol. 53; 1–15. https://doi.org/10.1016/j.jag.2016.08.007.

[16] Mutanga, O., Adam, E. and Cho, M. A., (2012). High Density Biomass Estimation for Wetland Vegetation Using WorldView-2 Imagery and Random Forest Regression Algorithm. *International Journal of Applied Earth Observation and Geoinformation*, Vol. 18(1); 399–406. https://doi.org/10.1016/j.jag.2012.03.012.

[17] Mutanga, O., Masenyama, A. and Sibanda, M., (2023). Spectral Saturation in the Remote Sensing of High-Density Vegetation Traits: A Systematic Review of Progress, Challenges, and Prospects. In *ISPRS Journal of Photogrammetry and Remote Sensing*, Vol. 198; 297–309. https://doi.org/10.1016/j.isprsjprs.2023.03.010.

[18] Nesha, M. K., Hussin, Y. A., van Leeuwen, L. M. and Sulistioadi, Y. B., (2020). Modeling and Mapping Aboveground Biomass of the Restored Mangroves using ALOS-2 PALSAR-2 in East Kalimantan, Indonesia. *International Journal of Applied Earth Observation and Geoinformation*, Vol. 91; 1-9. https://doi.org/10.1016/j.jag.2020.102158.

[19] Kaasalainen, S., Holopainen, M., Karjalainen, M., Vastaranta, M., Kankare, V., Karila, K. and Osmanoglu, B., (2015). Combining Lidar and Synthetic Aperture Radar Data to Estimate Forest Biomass: Status and Prospects. *Forests*, Vol. 6(1); 252–270. https://doi.org/10.3390/f6010252.

[20] Neka, W., (2019). Analisis Potensi Hutan Mangrove di Teluk Pangpang Banyuwangi Dalam Pengembangan Ekonomi Masyarakat Pesisir [Analysis of the Potential of Mangrove Forests in Pangpang Bay, Banyuwangi in the Economic Development of Coastal Communities]. *Jurnal Techno-Fish*, Vol. 3(1); 31-45. https://ejournal.unitomo.ac.id/index.php/perikanan/article/view/1762/871.

[21] Buwono, Y. R., (2017). Identifikasi dan Kerapatan Ekosistem Mangrove di Kawasan Teluk Pangpang Kabupaten Banyuwangi [Identification and Density of Mangrove Ecosystems in the Pangpang Bay Area, Banyuwangi Regency]. *Samakia: Jurnal Ilmu Perikanan*, Vol. 8(1); 32–37. http://samakia.aperiki.ac.id/index.php/JSAPI.

[22] Louis, J., Pflug, B., Main-Knorn, M., Debaecker, V., Mueller-Wilm, U., Iannone, R. Q., Cadau, E. G., Boccia, V. and Gascon, F., (2019). Sentinel-2 Global Surface Reflectance Level-A2 Product Generated with Sen2Cor. *2019 IEEE International Geoscience & Remote Sensing Symposium*. https://doi.org/10.1109/IGARSS.2019.8898540.

[23] Indriasari, N., Arief, R., Kustiyo, Budiono, M. E., Dyatmika, H. S., Rahayu, M. I., Payani, A. S., Amriya, Q., Maulana, R. and Ali, S., (2020). Analisa Filter Spekle Single dan Multitemporal Data Sentinel 1-A [Single and Multitemporal Speckle Filter Analysis of Sentinel 1-A Data]. *IOP Conference Series: Earth and Environmental Science*, Vol. 500(1). https://doi.org/10.1088/1755-1315/500/1/012021.

[24] Cheng, X., Naiara, P. and Gong, J., (2012). Terrain Radiometric Calibration of Airborne UAVSAR for Forested Area. *Geo-Spatial Information Science*, Vol. 15(4); 229–240. https://doi.org/10.1080/10095020.2012.745050.

[25] Small, D., (2011). Flattening Gamma: Radiometric Terrain Correction for SAR Imagery. *IEEE Transactions on Geoscience and Remote Sensing*, Vol. 49(8); 3081–3093. https://doi.org/10.1109/TGRS.2011.2120616.

[26] Park, J. W., Korosov, A. A., Babiker, M., Sandven, S. and Won, J. S., (2018). Efficient Thermal Noise Removal for Sentinel-1 TOPSAR Cross-Polarization Channel. *IEEE Transactions on Geoscience and Remote Sensing*, Vol. 56(3); 1555–1565. https://doi.org/10.1109/TGRS.2017.2765248.

[27] Filipponi, F., (2019). Sentinel-1 GRD Preprocessing Workflow. *3rd International Electronic Conference on Remote Sensing*, Vol. 11. https://doi.org/10.3390/ECRS-3-06201.

[28] Muhsoni, F. F., Sambah, A. B., Mahmudi, M. and Wiadnya, D. G. R., (2018). Comparison of Different Vegetation Indices for Assessing Mangrove Density Using Sentinel-2 Imagery. *International Journal of GEOMATE*, Vol. 14(45); 42–51. https://doi.org/10.21660/2018.45.7177.

[29] Vreugdenhil, M., Wagner, W., Bauer-Marschallinger, B., Pfeil, I., Teubner, I., Rüdiger, C. and Strauss, P., (2018). Sensitivity of Sentinel-1 Backscatter to Vegetation Dynamics: An Austrian Case Study. *Remote Sensing*, Vol. 10(9). https://doi.org/10.3390/rs10091396.

[30] Vreugdenhil, M., Navacchi, C., Bauer-Marschallinger, B., Hahn, S., Steele-Dunne, S., Pfeil, I., Dorigo, W., and Wagner, W., (2020). Sentinel-1 Cross Ratio and Vegetation Optical Depth: A Comparison Over Europe. *Remote Sensing*, Vol. 12(20); 1–19. https://doi.org/10.3390/rs12203404.

[31] Prakash, A. J., Behera, M. D., Ghosh, S. M., Das, A. and Mishra, D. R., (2022). A New Synergistic Approach for Sentinel-1 and PALSAR-2 in a Machine Learning Framework to Predict Aboveground Biomass of a Dense Mangrove Forest. *Ecological Informatics*, Vol. 72; 1-14. https://doi.org/10.1016/j.ecoinf.2022.101900.

[32] Nasirzadehdizaji, R., Sanli, F. B., Abdikan, S., Cakir, Z., Sekertekin, A. and Ustuner, M., (2019). Sensitivity Analysis of Multi-Temporal Sentinel-1 SAR Parameters to Crop Height and Canopy Coverage. *Applied Sciences*, Vol. 9(4). https://doi.org/10.3390/app9040655.

[33] Yu, H., Yang, Y., Wang, C., Chen, R., Xie, Q., Liu, G. and Yin, G., (2023). Extracting Deciduous Forests Spring Phenology from Sentinel-1 Cross Ratio Index. *IEEE Journal of Selected Topics in Applied Earth Observations and Remote Sensing*, Vol. 16; 2841–2850. https://doi.org/10.1109/JSTARS.2023.3247833.

[34] Rouse, J. W., Jr., Haas, R. H., Schell, J. A. and Deering, D. W., (1974). Monitoring Vegetation Systems in the Great Plains with ERTS. *Third Earth Resources Technology Satellite-1 Symposium, Washington, D.C*. 309-317.

[35] Huete, A., Didan, K., Miura, T., Rodriguez, E. P., Gao, X. and Ferreira, L. G., (2002). Overview of the Radiometric and Biophysical Performance of the MODIS Vegetation Indices. *Remote Sensing of Environment*, Vol. 83(1–2); 195-213. https://doi.org/10.1016/S0034-4257(02)00096-2.

[36] Clevers, J. P. W., (1986). The Application of a Vegetation Index in Correcting the Infrared Reflectance for Soil Background. *Symposium of Remote Sensing for Resource Development and Environment Management,* Enschede, The Netherland. 221-226.

[37] Huete, A., (1988). A Soil-Adjusted Vegetation Index (SAVI). *Remote Sensing of Environment*, Vol. 25; 295–309. https://doi.org/10.1016/0034-4257(88)90106-X.

[38] Qi, J., Chehbouni, A., Huete, A. R., Kerr, Y. H. and Sorooshian, S., (1994). A Modified Soil Adjusted Vegetation Index. *Remote Sensing of Environment*, Vol. 48; 119–126. https://doi.org/10.1016/0034-4257(94)90134-1.

[39] Kaufman, Y. J. and Tanre, D., (1992). Atmospherically Resistant Vegetation Index (ARVI) for EOS-MODIS. *IEEE Transactions on Geoscience and Remote Sensing*, Vol. 30(2); 261-270. https://doi.org/10.1109/36.134076.

[40] Purnamasari, E., Kamal, M. and Wicaksono, P., (2021). Comparison of Vegetation Indices for Estimating Above-Ground Mangrove Carbon Stocks Using Planetscope Image. *Regional Studies in Marine Science*, Vol. 44; 1-8. https://doi.org/10.1016/j.rsma.2021.101730.

[41] Komiyama, A., Poungparn, S. and Kato, S., (2005). Common Allometric Equations for Estimating the Tree Weight of Mangroves. *Journal of Tropical Ecology*, Vol. 21(4); 471–477. https://doi.org/10.1017/S0266467405002476.

[42] Komiyama, A., Ong, J. E. and Poungparn, S., (2008). Allometry, Biomass, and Productivity of Mangrove Forests: A Review. *Aquatic Botany*, Vol. 89(2); 128–137. https://doi.org/10.1016/j.aquabot.2007.12.006.

[43] Suardana, A. A. M. A. P., Anggraini, N., Nandika, M. R., Aziz, K., As-syakur, A. R., Ulfa, A., Wijaya, A. D., Prasetio, W., Winarso, G. and Dewanti, R., (2023). Estimation and Mapping Above-Ground Mangrove Carbon Stock Using Sentinel-2 Data Derived Vegetation Indices in Benoa Bay of Bali Province, Indonesia. *Forest and Society*, Vol. 7(1); 116–134. https://doi.org/10.24259/fs.v7i1.22062.

[44] Shu, Q., Xi, L., Wang, K., Xie, F., Pang, Y. and Song, H., (2022). Optimization of Samples for Remote Sensing Estimation of Forest Aboveground Biomass at the Regional Scale. *Remote Sensing*, Vol. 14(17). https://doi.org/10.3390/rs14174187.

[45] Roscoe, J. T., (1975). *Fundamental Research Statistics for the Behavioral Sciences*. New York: Holt, Rinehart and Winston.

[46] Jiang, J., (2022). Simple Linear Correlation. In *Applied Medical Statistics*. Oxford, UK: John Wiley and Sons, Inc. 331–344. https://doi.org/10.1002/9781119716822.ch14

[47] Taylor, B. M., (2020). A Multi-Way Correlation Coefficient. *ArXiv: Methodology*. https://doi.org/10.48550/arXiv.2003.02561.

[48] Piepho, H. P., (2023). An Adjusted Coefficient of Determination (R^2) For Generalized Linear Mixed Models in One Go. *Biometrical Journal*, Vol. 65(7); 1-17. https://doi.org/10.1002/bimj.202200290.

[49] David, R. M., Rosser, N. J. and Donoghue, D. N. M., (2022). Improving Above Ground Biomass Estimates of Southern Africa Dryland Forests by Combining Sentinel-1 SAR and Sentinel-2 Multispectral Imagery. *Remote Sensing of Environment*, Vol. 282. https://doi.org/10.1016/j.rse.2022.113232.

[50] Siegel, A. F., (2016). Correlation and Regression: Measuring and Predicting Relationships. Practical Business Statistics, 7th ed., A. F. Siegel, Ed. London, UK: Academic Press, 2016, 299-354. https://doi.org/10.1016/B978-0-12-804250-2.00011-0.

[51] Nattino, G., Finazzi, S. and Bertolini, G., (2016). A New Test and Graphical Tool to Assess the Goodness of Fit of Logistic Regression Models. *Statistics in Medicine*, Vol. 35(5); 709–720. https://doi.org/10.1002/sim.6744.

[52] Malik, A. H. and Devi, R. U., (2022). An Update on the Remote Sensing Applications for Sustainable Coastal Management. *Disaster Advances*, Vol. 15(9); 40–49. https://doi.org/10.25303/1509da040049.

[53] Zhao, P., Lu, D., Wang, G., Wu, C., Huang, Y. and Yu, S., (2016). Examining Spectral Reflectance Saturation in Landsat Imagery and Corresponding Solutions to Improve Forest Aboveground Biomass Estimation. *Remote Sensing*, Vol. 8(6). https://doi.org/10.3390/rs8060469.

[54] Hidayah, Z., Rachman, H. A. and Wiyanto, D. B., (2024). Assessment of Spatio-Temporal Dynamics of Mangrove Forest in Teluk Pangpang, Banyuwangi, East Java, Indonesia. *Biodiversitas*, Vol. 25(7); 3138–3150. https://doi.org/10.13057/biodiv/d250736.

[55] Pham, T. D., Yokoya, N., Bui, D. T., Yoshino, K. and Friess, D. A., (2019). Remote Sensing Approaches for Monitoring Mangrove Species, Structure, and Biomass: Opportunities and Challenges. *Remote Sensing*, Vol. 11(3). https://doi.org/10.3390/rs11030230.

[56] Sims, D. A. and Gamon, J. A., (2002). Relationships Between Leaf Pigment Content and Spectral Reflectance Across a Wide Range of Species, Leaf Structures and Developmental Stages. *Remote Sensing of Environment*, Vol. 81(2–3); 337–354. https://doi.org/10.1016/S0034-4257(02)00010-X.

[57] Ronoud, G., Fatehi, P., Darvishsefat, A. A., Tomppo, E., Praks, J. and Schaepman, M. E., (2021). Multi-Sensor Aboveground Biomass Estimation in the Broadleaved Hyrcanian Forest of Iran. *Canadian Journal of Remote Sensing*, Vol. 47(6); 818–834. https://doi.org/10.1080/07038992.2021.1968811.

[58] Li, J., (2017). Assessing the Accuracy of Predictive Models for Numerical Data: Not *r* nor r^2, why not? Then what? *PLoS ONE*, Vol. 12(8). https://doi.org/10.1371/journal.pone.0183250.

[59] Kamal, M., Hidayatullah, M. F., Mahyatar, P. and Ridha, S. M., (2022). Estimation of Aboveground Mangrove Carbon Stocks from WorldView-2 Imagery Based on Generic and Species-Specific Allometric Equations. *Remote Sensing Applications: Society and Environment*, Vol. 26. https://doi.org/10.1016/j.rsase.2022.100748.

[60] Candra, E. D., Hartono, and Wicaksono, P., (2016). Above Ground Carbon Stock Estimates of Mangrove Forest Using WorldView-2 Imagery in Teluk Benoa, Bali. *IOP Conference Series: Earth and Environmental Science*, Vol. 47(1). https://doi.org/10.1088/1755-1315/47/1/012014.